THE JOURNAL OF PHYSICAL CHEMISTRY C

Article

pubs.acs.org/JPCC

Role of Host–Guest Interactions in Tuning the Optical Properties of Coumarin Derivatives Incorporated in MCM-41: A TD-DFT Investigation

Alfonso Pedone,*[,†] Julien Bloino,[‡,§] and Vincenzo Barone[§]

[†]Dipartimento di Scienze Chimiche e Geologiche, Università di Modena e Reggio Emilia, via G. Campi 183, I-41125 Modena, Italy

[‡]Consiglio Nazionale delle Ricerche, Istituto di Chimica dei Composti OrganoMetallici (ICCOM-CNR), UOS di Pisa, Area della Ricerca, via G. Moruzzi 1, I-56124 Pisa, Italy

[§]Scuola Normale Superiore, Piazza dei Cavalieri 7, I-56126 Pisa, Italy

Supporting Information

ABSTRACT: The encapsulation of organic dye molecules in silica-based nanostructures leads to composite materials with novel optical properties and a wide range of applications in the field of nanotechnology. The design of new dye-doped silica-based devices requires a deep understanding of how host–guest interactions affect the optical properties and stability of the dye/silica assembly. In this work, density functional theory (DFT) and time-dependent DFT (TD-DFT) calculations have been employed to investigate the effect of the host–guest interactions on the structural, optical, and electronic properties of two 7-aminocoumarin dyes (labeled C339 and C340) incorporated into MCM-41. Our calculations show that the interaction of the carbonyl groups of the coumarin molecules with the silanol groups on the silica surface is responsible for the dye stabilization and is strengthened upon photoexcitation. As a result, the computed absorption and emission spectra of the incorporated dyes are red-shifted compared to those in toluene, in perfect agreement with experimental measurements. The computed electronic spectra reproduce well both the solvatochromic and Stokes shifts of the dye molecule in toluene and MCM-41, and also, the band-shape can be reconstructed by simply including the vibrational fine structure associated to the electronic transition.

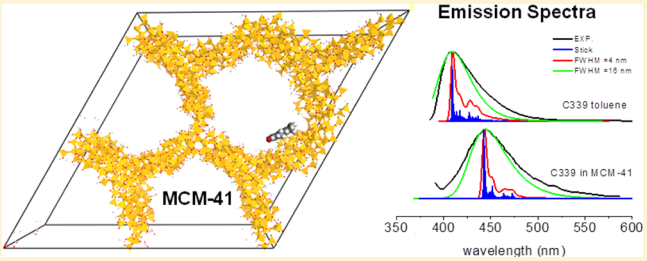

INTRODUCTION

Dye-doped silica nanoarchitectures have proved to exhibit various optical properties for a wide range of potential applications, such as sensors, lasers, frequency doublers, optical switches, limiters, amplifiers, or storage devices, as well as solar concentrators.[1]

Several studies have shown that the embedding of functional chromophores in sol–gel-derived nanoparticles and zeolites leads to a strong increase in photostability compared to organic polymeric matrixes. Indeed, the more rigid environment hampers in many cases photobleaching and fluorescence quenching and thus increases photostability and brightness.[1,2] After the discovery of mesoporous molecular sieves,[3] several dye molecules have been incorporated into MCM-41,[4−6] a mesoporous architecture, which possesses a well-ordered porous structure with uniform hexagonal mesopores of diameter ranging from 1.5 to 10 nm and favors the entrapment of large organic dyes with respect to zeolites. Several previous studies revealed that the strong dye/MCM-41 interaction increased the lifetime of the dye molecules when incorporated into the silica mesoporous material and reduced their aggregation at high concentration.[7] These findings have paved the route toward the design of new solid-state dye lasers possessing several advantages such as compactness, high potential for miniaturization, absence of toxic solutions, safe handling, and disposal of spent laser media with respect to solvent-based dye lasers.[1] Among the different dye lasers, coumarin derivatives having an amino substituent at position 7 have shown to be of special significance in relation with their laser activity, but the type of host largely determines the laser performance.[5,6]

Therefore, a deeper understanding of host–guest interactions is crucial for the design of the aforementioned devices since the optical properties of the entrapped dyes strongly depend on the chemical interactions with the silanol groups and the physical interactions with the cage walls present in porous silica nanostructures. Electronic absorption and emission spectra of dye-doped silica-based nanoarchitectures are excellent methods to study the influence of the environment on electronic states and the strength of host–guest interactions since the guest molecule can be regarded as an inherent probe of the hosting structure.

Received: May 31, 2012
Revised: July 10, 2012
Published: July 30, 2012

However, the interpretation of the rich indirect information that can be inferred from the analysis of experimental spectra is seldom straightforward because of the subtle interplay of different effects, such as those coming from the nuclear motions (vibrational effects) and those depending on the surrounding environment. The specific role of each effect is not easy to individuate and evaluate, and this calls for adequate interpretative tools, especially in condensed phases.

In such scenarios, the development and validation of effective tools for the prediction and interpretation of electronic absorption and fluorescence spectra is extremely useful, and significant progress has been made in the past few years.[8−13]

Several integrated approaches have been employed to investigate very complex systems by combining quantum mechanical (QM) calculations rooted in density functional theory (DFT) and its time-dependent extension (TD-DFT)[14] with classical molecular mechanics (MM) and the polarizable continuum model (PCM),[15] using localized basis sets.[12,16−19] Those QM/MM/PCM techniques can be used in the framework of both time-independent and time-dependent approaches to dissect short-term dynamical effects in vacuum, as well as embedded in different environments.[20] Recently, we employed a time-dependent approach, which combines classical molecular dynamics simulations based on purposely tailored force-fields and TD-DFT quantum mechanical calculations to simulate the absorption and emission spectra and to elucidate the mechanisms behind the brightness enhancement of realistic models of rhodamine (TRITC)-based C-dots for the first time.[12,13]

The time-dependent route is particularly well-suited for flexible systems propagating on highly anharmonic potential energy surfaces (PES) with large-amplitude motions or solvent librations,[21,22] but it does not offer a detailed description of the manifold of individual transitions leading to the whole vibrationally resolved electronic spectra. The latter can be obtained by employing time-independent approaches, which are highly effective with semirigid molecular systems undergoing a limited modification of their structure upon the electronic transition.[10]

In this article, we present a detailed theoretical investigation of the effect of host−guest interactions on the optical and electronic properties of the two 7-aminocoumarin dyes shown in Figure 1 adsorbed on a realistic model of silica surface that can represent the walls of MCM-41.

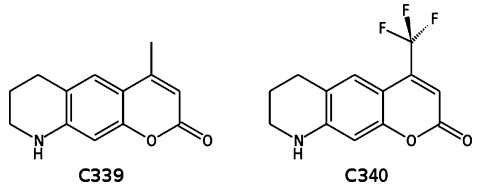

C339 C340

Figure 1. Chemical structures of the two coumarin derivatives considered.

Our final aim is to describe the physical−chemical properties of this assembly, which have not been theoretically studied to date, and to analyze how they control the observed spectroscopic features.

To understand the effects of the dye/MCM-41 interactions on the electronic and optical properties, we have calculated the binding energies and structural properties for both the ground- and excited-state relaxed geometries and the pure-electronic and vibrationally resolved absorption and emission spectra of the coumarin/silica assemblies using DFT and TD-DFT calculations in the time-independent framework.

COMPUTATIONAL DETAILS

Electronic Calculations and Environmental Effects. Two different coumarin derivatives have been considered in this work; 4-methyl-6,7,8,9-tetrahydro-pyrano[3,2-*g*]quinolin-2-one (commonly referred to as coumarin 339, noted C339 hereafter) and 4-trifluoromethyl-6,7,8,9-tetrahydro-pyrano[3,2-*g*]quinolin-2-one (C340). The two molecules, which are shown in Figure 1, differ by the presence of a $-CH_3$ (C339) or a $-CF_3$ (C340) substituent in position 6.

We have investigated the equilibrium structures of the ground and excited states, the charge distributions, and the absorption and emission electronic spectra of these molecules in vacuum, in toluene, and interacting with MCM-41.

All QM calculations were performed at the DFT and/or TD-DFT level of theory with a locally modified version of the Gaussian09 suite,[23] by employing the hybrid exchange−correlation functional B3LYP[24,25] coupled to the polarized double-ζ N07D basis set.[26] This basis set has been constructed by adding a reduced number of polarization and diffuse functions to the 6-31G set, which leads to an accuracy at least comparable to the aug-cc-pVDZ basis set, at a lower computational cost.

The pure electronic absorption and emission spectra were simulated by performing vertical $S_1 \leftarrow S_0$ and $S_1 \rightarrow S_0$ transitions from the ground- and the excited-state optimized geometries, respectively.

Environmental effects have been taken into account by employing the so-called polarizable continuum model (PCM), which has emerged in the last two decades as one of the most effective tools to treat bulk solvent effects for both ground- and excited-state properties.[15,27−29] In PCM, the solvent is described as a homogeneous dielectric medium, which is polarized by the solute. The latter is placed within a cavity in the solvent (built as the envelope of spheres centered on the solute atoms) and the proper electrostatic problem at the cavity surface is solved using a boundary element approach. Since the excitation of electrons and the radiative de-excitation (fluorescence) processes are intrinsically dynamical, it is important to take into account the characteristic times of the solvent's degrees of freedom. Within the PCM approach, the simplest, and the most commonly used, treatment involves the definition of two limit time regimes, the equilibrium (EQ) and the nonequilibrium (NEQ) one. In the former, all the solvent degrees of freedom are in equilibrium with the electron density of the solute, while in the latter, only the solvent electronic polarization is in equilibrium with the excited-state electron density. Therefore, NEQ-PCM is more suitable for the calculation of absorption processes in solution, while EQ-PCM is the method of choice for the investigation of excited-state structural relaxation processes. Another issue that arises when continuum models are applied to include environmental effects in the investigation of absorption and emission problems is that the solvent reaction field should be variationally determined together with all the other parameters in the electronic method used (i.e., MOs and CIs coefficients) since these parameters depend on the solvent reaction field itself. Two approaches are usually employed, that is the state-specific (SS) and linear-response (LR) approaches.[30,31]

In the SS method, a different effective Schrödinger equation is solved for each state of interest, achieving a fully variational formulation of solvent effects on the excited-state properties. In the LR formalism, the excitation energies are directly determined without computing the exact excited electron density, including a PCM correction, which typically depends on the electron density variation associated to the ground-to-excited-state transition.

In this work, the investigations on the two coumarin dyes in toluene have been carried out by employing the NEQ-LR-PCM approach for absorption processes and the EQ-SS-PCM approach for the emission ones. This method reproduces well solvent effects when no specific interaction (such as hydrogen bonds) takes place between the solute and the solvent molecules. When this is not the case, as in the coumarin dyes encapsulated in MCM-41, the best compromise is represented by mixed models, where all atoms involved in the interactions (i.e., the first solvation shell) are explicitly considered in the electronic calculations and then embedded in a second MM layer or in PCM to simulate bulk effects.[12,32]

Figure 2 shows the structural model generated to investigate the dye/MCM-41 interactions. We started from the structural model of the MCM-41 recently proposed by Ugliengo et al.,[33] whose unit cell contains 579 atoms ($Si_{142}O_{335}H_{102}$) and a tetrahedral-site density of 8.2 T-sites/1000 Å^3. A 2 × 2 × 2 supercell was created, and the two coumarin molecules were docked on the wall of the MCM-41 model as shown in the same figure.

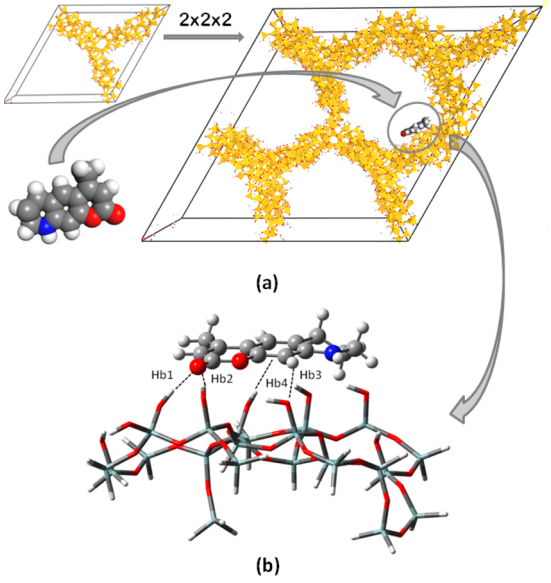

Figure 2. Representation of the cumarin/silica assembly used in all the calculations. (a) From the MCM-41 unit cell optimized at the B3LYP level by Ugliengo et al., a supercell 2 × 2 × 2 has been created and the coumarin dyes docked onto a silica wall. (b) Then, a cluster containing the coumarin dye (29 atoms) plus two layers of the silica tetrahedral (containing 94 atoms) interacting with it has been cut out from the whole system.

To study the dye/silica interaction at the QM level, a coumarin/silica assembly containing 123 atoms (29 of which are those of the coumarin dyes) has been extracted from the whole model and surrounded by the PCM with the silica dielectric constants (ε_0 = 3.8 and ε_∞ = 2.12).[34] To saturate the slab, hydrogen atoms were added to the extremities of the severed bonds. The geometry was then relaxed, keeping those terminal hydrogens fixed.

This approach is, in our opinion, the most consistent one for the calculations performed in toluene and the only one that allows us to carry out frequency calculations in both electronic states, needed to generate the vibrationally resolved electronic spectra (see next paragraph) of the dye molecules in toluene solution and interacting with the silica wall of MCM-41.

Our results will be compared with recent experimental data reported by Li et al.,[6] who have studied the effect of dye/silica interactions on the optical properties of the C339 and C340 coumarin dyes by measuring the absorption and emission spectra of these molecules in toluene and within MCM-41. In the latter case, the dye molecules were incorporated into calcined MCM-41 by impregnation of solutions of the dyes in toluene. The samples were then vacuumed and dried to remove the solvent. Therefore, no water molecule could mediate the dye/silica interaction, which makes our results directly comparable to those provided by Li and co-workers.

Vibrationally Resolved Electronic Spectra. While the standard, purely electronic approximation of the UV−visible spectrum gives a first insight of the spectrum observed experimentally, it remains a crude approximation to the rich structure of the latter. In order to improve the accuracy of the theoretical spectrum, it is necessary to include the vibrational fine structure associated to the electronic transition. The ensemble is often referred to as vibrationally resolved electronic spectroscopy, also known as vibronic spectroscopy. In order to generate a vibronic spectrum, it is necessary to know the potential energy surface (PES) of both electronic states involved in the transition. An extensive sampling of the PES is impossible for all molecular systems but the smallest ones. In order to treat medium-to-large systems, the PES is approximated harmonically, through the calculation of the Hessian matrixes. This simplification is problematic when the minima of the 2 PESs are shifted. Indeed, the correct description of the vertical transition would require to compute the force constants of the final state's PES about the equilibrium geometry of the initial one. This approach, which can be referred to as vertical Hessian,[35,36] reproduces well the most intense bands of the spectrum, but since the relative positions of the minima of the PESs are not known and the frequencies are approximated, the position of the bands can be offset and the fine structure of the spectrum incorrectly represented. An alternative strategy, referred to as adiabatic Hessian,[37−42] treats both electronic states on the same footing by using the force constants computed about the respective minimum of each PES. This offers a consistent description of the band-shape, albeit the most intense bands can be less accurately reproduced than in the vertical model. For this reason, the latter model has been employed in the present study. It should be noted that both models give equal results when there is no shift between the minima of the 2 PESs.

The one-photon absorption (OPA) and emission (OPE) spectra have been generated by computing the molar extinction coefficient $\varepsilon(\omega)$ and the energy emitted by one mole per second I_{em}:[10]

$$\varepsilon(\omega) = \frac{10\pi N_A}{3\varepsilon_0 \ln(10)\hbar c} \times \sum_i \rho_i \sum_f |\langle\Psi_i|\hat{\mu}|\Psi_j\rangle|^2 \times \delta(E_f - E_i - \hbar\omega) \quad (1)$$

dx.doi.org/10.1021/jp305294u | J. Phys. Chem. C 2012, 116, 17807−17818

Table 1. Optimized Geometry of the Ground State (S_0) and First Excited State (S_1) of coumarins 339 and 340 in toluene and adsorbed in MCM-41

	coumarin 339				coumarin 340			
	toluene		MCM-41		toluene		MCM-41	
	S_0	S_1	S_0	S_1	S_0	S_1	S_0	S_1
				Bond Lengths (Å)				
1	1.21	1.23	1.23	1.25	1.21	1.23	1.23	1.25
2	1.39	1.43	1.37	1.41	1.39	1.42	1.36	1.39
3	1.36	1.36	1.37	1.36	1.37	1.36	1.38	1.37
4	1.41	1.43	1.41	1.41	1.41	1.41	1.42	1.40
5	1.45	1.45	1.44	1.48	1.44	1.48	1.43	1.48
6	1.36	1.40	1.37	1.39	1.36	1.39	1.37	1.39
7	1.45	1.42	1.44	1.42	1.46	1.43	1.44	1.42
8	1.49	1.49	1.50	1.49	1.52	1.47	1.52	1.48
9	1.39	1.38	1.38	1.40	1.39	1.39	1.38	1.40
10	1.40	1.42	1.41	1.42	1.41	1.41	1.41	1.42
11	1.41	1.42	1.43	1.41	1.43	1.42	1.43	1.42
12	1.39	1.40	1.38	1.40	1.38	1.39	1.38	1.39
13	1.41	1.42	1.42	1.42	1.41	1.41	1.42	1.42
14	1.38	1.37	1.37	1.37	1.37	1.37	1.36	1.36
15	1.46	1.46	1.46	1.45	1.46	1.46	1.46	1.46
16	1.53	1.53	1.53	1.53	1.53	1.53	1.53	1.53
17	1.54	1.54	1.54	1.54	1.53	1.54	1.54	1.54
18	1.52	1.51	1.51	1.51	1.52	1.51	1.51	1.51
				Bond Angles (deg)				
A	116.1	116.5	117.8	117.4	116.0	117.0	117.9	118.3
B	122.5	121.3	122.1	120.3	123.1	121.0	122.7	120.4
C	121.5	122.3	120.9	123.4	121.5	123.4	120.8	123.5
D	118.1	118.6	118.4	118.2	116.7	117.4	116.9	117.2
E	118.8	116.9	118.9	116.0	121.0	117.2	121.1	117.3
F	123.0	124.5	122.2	124.7	121.6	124.0	120.6	123.3
G	121.9	121.3	122.6	121.0	122.0	121.2	122.7	121.4
H	120.1	120.0	119.7	119.9	120.0	120.0	119.6	119.7
I	119.6	120.5	119.6	121.0	119.6	120.3	119.5	120.5
L	118.6	118.0	118.9	117.2	118.9	117.9	119.1	117.7
M	123.0	122.9	122.8	123.5	122.7	123.1	122.5	123.3
N	116.8	117.2	116.4	117.4	117.0	117.6	116.5	117.4
O	120.3	120.5	120.4	121.2	120.3	120.4	120.4	120.9
P	122.3	123.2	124.4	123.3	123.2	123.6	124.5	123.9
Q	109.6	110.2	110.7	110.7	109.9	110.5	110.4	110.7
R	110.0	110.3	109.5	110.2	110.0	110.4	109.7	110.2
S	111.7	111.5	110.4	110.7	111.5	111.2	110.6	110.5
T	119.7	119.7	118.1	119.0	119.4	119.6	118.2	118.6
				Improper Angle (deg)				
nitrogen	162.0	172.8	179.0	178.5	169.0	174.9	179.0	179.8

$$I_{em} = \frac{2N_A\omega^4}{3\varepsilon_0 c^3} \times \sum_i \rho_i \sum_f |\langle \Psi_i|\hat{\mu}|\Psi_j\rangle|^2 \times \delta(E_f - E_i + \hbar\omega) \quad (2)$$

The double summation runs over all initial (i) and final (f) states. ρ_i is the Boltzmann population of initial vibrational state i, N_A the Avogadro number, and ε_0 the vacuum permittivity. Ψ_i and Ψ_f are the molecular wave functions of the initial and final states, respectively.

Details about the procedure used to compute vibronic spectra can be found in refs 8 and 10. Here, we will focus on some features of particular interest for the present treatment. A first issue lies in the absence of analytic formulation of the electronic transition dipole moment between the initial and final states, $\boldsymbol{\mu}_{if}^{e}$. This is generally overcome by performing a Taylor expansion with respect to a set of normal coordinates $\mathbf{Q}$ about the equilibrium geometry of the initial (vertical Hessian model) or final (adiabatic Hessian) states:

$$\boldsymbol{\mu}_{if}^{e} \approx \boldsymbol{\mu}_{if}^{e}(\mathbf{Q}_{eq}) + \sum_{k=1}^{N} \frac{\partial \boldsymbol{\mu}_{if}^{e}}{\partial \mathbf{Q}_k}\mathbf{Q}_k \quad (3)$$

The 0th order corresponds to the Franck−Condon (FC) approximation and is generally sufficient to treat fully allowed electronic transitions for one-photon processes. The first-order term is the Herzberg−Teller (HT) approximation, which accounts for an intensity-borrowing effect from electronic states close to those involved in the transition and is dominant in weakly allowed or dipole-forbidden transitions. Inclusion of both terms in the right-hand side of eq 3 is labeled FCHT.

To compute the vibrational overlap integrals, the Duschinsky transformation is used to express the normal coordinates of the

dx.doi.org/10.1021/jp305294u | J. Phys. Chem. C 2012, 116, 17807−17818

initial electronic state Q' with respect to those of the final state Q'':

$$\mathbf{Q}' = \mathbf{J}\mathbf{Q}'' + \mathbf{K} \quad (4)$$

where $\mathbf{J}$ is the Duschinsky matrix and $\mathbf{K}$ is the shift vector due to the changes in geometry; $J = L'^{T}L''$, $K = L'^{T}M^{1/2}\Delta X$: L' and L'' are, respectively, the transformation matrixes from mass-weighted Cartesian coordinates to normal coordinates of the initial and final states, $\mathbf{M}$ is the diagonal matrix of atomic masses, $\Delta\mathbf{X}$ is a vector representing the shift of nuclear coordinates between the initial and final states. It should be noted that, in the calculations, the real Duschinsky matrix is used.

Finally, we should comment about the practical treatment of the double summation over all initial and final vibrational states in eqs 1 and 2, which is in principle infinite. At 0 K, the sum over the initial states vanishes. Since only a limited number of transitions contributes significantly to the band-shape, a class-based prescreening method is used to select a priori those transitions, which are then taken into account in the actual summation. For higher temperatures, the initial states are included in the summation based on their Boltzmann population. In practice, the minimum population is calculated with respect to the ground state, and a maximum number of simultaneously excited modes is chosen to keep the computational cost affordable. The initial states are grouped by sets depending on which modes are excited (same number and same modes). For each set, the prescreening method is applied to choose the most intense transitions.

To compute the vibronic spectra, we performed geometry optimizations followed by frequency calculations for both ground and first excited states. Since frequency calculations for the excited state are performed at the TDDFT level by numerical differentiation of analytical forces, this step has a high computational cost, which can quickly become prohibitive for large systems. For this reason, we have focused our study on vibrationally resolved electronic spectra on coumarin 339. Geometry optimizations and frequency calculations of C339 in toluene were done with a purely implicit solvent, as described previously. The system composed of coumarin adsorbed on the slab shown in Figure 2b represents a more challenging task, especially to obtain the frequencies. Since C339 is the photoactive compound in the whole system, it is possible to reduce the computational cost with limited impact on the reliability of the results by keeping the atoms from the slab fixed while computing the harmonic force constants in the initial and final states from the relaxed structures obtained as described above. In order to validate this reduced-dimensionality scheme, a comparison between this model and the full system is presented in the Supporting Information. The analysis is based on a projection of their respective normal coordinates, using those of the full system as reference, in a similar way to the Duschinsky transformation. Figure S1 of the Supporting Information shows the projection of the normal modes of the C339 molecule for the reduced system on the normal modes of the full system, while Figure S2 shows the correlation between the vibrational frequencies associated to the intramolecular normal modes of the C339 molecule for the two systems. The excellent match hints at a negligible impact of the vibrations of the atoms of the silica slab on those of the coumarin, so that our approximation can be safely employed. The results obtained for the ground state have been assumed to stand in the excited state, so that the model was used to compute frequencies in both electronic states.

RESULTS AND DISCUSSIONS

Ground State and Excited State Properties of C339 and C340 in Toluene and MCM-41. The intramolecular geometric parameters (bond lengths and bond angles) of the optimized ground and first excited state structures of C339 and C340 are listed in Table 1. Figure 3 shows the molecular structure designation, in particular, the bonds are designed by numbers (1−18) and the bond angles are designed by letters (A−T).

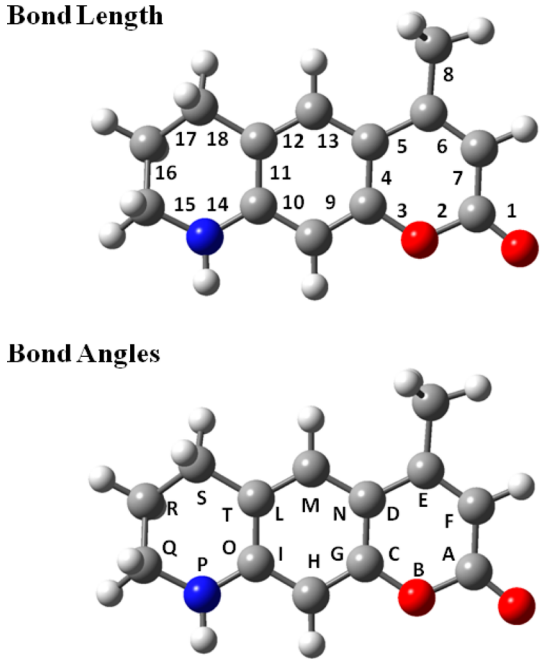

Figure 3. Designation of bonds and bond angles of C339 and C340.

As seen in the table, the structures of both molecules in toluene are very similar and photoabsorption induces only minor structural changes because of the rigid backbone of the molecule. In the ground state, the bond lengths of the central aromatic rings are intermediate between single and double C−C bonds ranging from 1.39 to 1.41 Å, while bonds 2 to 7 show large bond alternations ranging from 1.36 to 1.45 Å.

In the excited state, the central aromatic rings show a lengthening of the bonds and bond alternation, between 1.38 and 1.43 Å. Conversely, bond-length alternation is reduced for bonds numbered 5, 6, and 7. In particular, while the length of bonds 6, 7, and 1 are 1.36, 1.45, and 1.21 Å in the ground state, confirming an alternation between a double C═C (6), a quasi-single C−C (7), and a major double C═O (1) bond, the three bond lengths are 1.40, 1.42, and 1.23 Å in the excited state, respectively.

Table 1 shows that the bond angles of the two coumarin dyes, both in toluene and in MCM-41, are very similar with differences within 2°. However, by looking at the improper dihedral angle of the nitrogen atom, it is evident that the amino group of C339 in the ground state has a pyramidal structure (improper dihedral angle of 162°), while in the excited-state optimized structure, the amino group is slightly more planar (angle of 173°). Interestingly, when the molecule is adsorbed

dx.doi.org/10.1021/jp305294u | J. Phys. Chem. C 2012, 116, 17807−17818

on MCM-41, the amino group is planar in both the ground and excited states.

As for C340, the amino group is slightly more planar than C339 in toluene in both electronic states and is planar when adsorbed on MCM-41.

Table 1 also shows that the structures of C339 and C340 are not heavily deformed when the molecules interact with the silica matrix, the major changes occurring for the C═O bond length, which increases by 0.02 Å. This is due to the formation of two strong H-bonds between the C═O moiety and two silanol groups at the silica surface. These H-bonds are labeled Hb1 and Hb2 in Figure 2b, which shows the optimized C339/silica assembly. The Hb3 bond involves an aromatic H atom of the central ring and the O atom of a silanol group at the silica surface while Hb4 arises from the interaction between the electron density on the aromatic ring and the positive H atom of a silanol group. The latter interaction is similar to a cation−π interaction.

The distances of the four H-bonds previously described for both C339 and C340 in both the ground- and excited-state structures are reported in Table 2. The table shows that, in the ground state, Hb1 and Hb2 range from 1.79 to 1.82 Å, while Hb3 and Hb4 are longer and range from 2.23−2.28 to 2.50−2.55 Å, respectively.

Table 2. H-Bond Distances and Bonding Energies of C339 and C340 Adsorbed in MCM-41

	C339		C340	
	S_0	S_1	S_0	S_1
Hb1	1.79	1.73	1.82	1.76
Hb2	1.81	1.75	1.82	1.77
Hb3	2.28	2.20	2.23	2.16
Hb4	2.50	2.45	2.55	2.50
BE (kcal/mol)	9.9	14.4	7.5	13.1

The H-bond distances decrease when the dye molecules are in their first excited state. In particular, the lengths of both the Hb1 and Hb2 intermolecular hydrogen bonds are remarkably shortened in the excited state in comparison with those in the ground state. This indicates that the two H-bonds between the carbonyl group and the silanol groups are significantly strengthened. This is consistent with other theoretical studies of the electronic excited state hydrogen bonding dynamics for coumarins in water solution.[43−45]

The strength of the interaction between the coumarin molecules and the silica surface is measured by the binding energies (BE) reported in Table 2, which were computed as the difference between the isolated silica shell and adsorbate energies and the total energy of the combined adsorbate/substrate system. In all calculations, the basis set superposition error (BSSE) correction has been taken into account. The BE of the C339/silica assembly increases from 9.9 to 14.4 kcal/mol for the ground- and the first excited-state optimized configurations, while the BE of the C340/silica assembly increases from 7.5 to 13.1 kcal/mol so the C340 molecule seems to interact less with the silica surface. Thus, the intermolecular hydrogen bonding interactions for both C339 and C340 are strengthened in the electronic excited states. Those conclusions are also supported by analysis of the changes in length of the H-bonds.

Some insights into charge reorganizations issuing from electronic excitations can be obtained by analyzing the Mulliken charges of the backbone of C339 and C340 both in the ground and in the excited electronic states, in toluene solution, and in MCM-41. These results are shown in Figure 4, where the Mulliken charges reported in parentheses are those calculated for the first excited state. The Mulliken charge of the nitrogen atom in C339 in toluene solution increases from −0.49 in the ground state to −0.42 in the excited state, while the electron density of the atoms of the ring containing the lactonic moiety increase upon absorption of light; for example, the charge of the carbonyl oxygen decreases from −0.60 to −0.68. As a result, the electric dipole moment increases from 7.7 to 14.4 D upon excitation. This is a well-known phenomenon that leads to large solvent and Stokes shifts, two properties that make coumarin derivatives probably the most used molecular probes for investigating solvation dynamics. A similar charge redistribution effect is seen for C340. However, the electron-withdrawing CF_3 group subtracts electrons from the carbonyl group and the atoms nearby. In this case, the electric dipole moment changes from 7.8 to 15.3 D for the ground and the first excited state, respectively. Conversely, the Mulliken charges of the atoms in the aromatic rings and of those of the ring containing the nitrogen atom are slightly affected when the two molecules are adsorbed in MCM-41. Indeed, the formation of two hydrogen bonds between the carbonyl group of the dyes and the silanol groups of the silica surface stabilizes the more ionic resonance structure of the carbonyl group, which bear charges close to + and −1 for the C and O atoms, respectively.

Absorption and Emission Electronic Spectra of C339 and C340 in Toluene and MCM-41. The absorption ($S_1 \leftarrow S_0$) and emission ($S_1 \rightarrow S_0$) transition energies of C339 and C340 in vacuum, in toluene solution, and adsorbed in MCM-41 are reported in Table 3, together with their experimental counterparts previously published by Li et al.[6] Table 3 shows that the excitation energies of the C339 and C340 coumarin dyes within MCM-41 are red-shifted by about 22 and 24 nm with respect to those in toluene, in close agreement with the experimental values of 24 and 23 nm, respectively. Analysis of the computed singlet excited state shows that the lower energy absorption is due to the first dipole-allowed $\pi \rightarrow \pi^*$ transition with the largest oscillator strength from the highest occupied molecular orbital (HOMO) to the lowest unoccupied molecular orbital (LUMO). Figure 5 shows these Kohn−Sham orbitals for coumarins 339 and 340 in toluene solution. Similar shapes of the frontier orbitals have been found also in MCM-41. Figure 6 shows that these MOs remain localized on the dye molecules and the contribution of the silica surface to the absorption spectra is dominated by purely electrostatic interactions. Figure 5 shows also the electron density difference between the excited and the ground states upon light absorption, the dark violet clouds representing positive regions (regions in which the electron density increases during the transition) and the light green clouds negative regions (in which the electron density decreases during the transition). It can be clearly noted that the electron density on the carbonyl moiety is enhanced at the expense of the electron density on the amine group after the orbital transition from HOMO to LUMO. This further indicates that the intermolecular H-bonds between the C═O and the H−O groups are strengthened upon photoexcitation.

The calculated emission energies reported in Table 3 for C339 and C340 in MCM-41 are also in good agreement with experimental findings, being red-shifted with respect to their counterparts simulated in toluene solution by about 43 nm (the

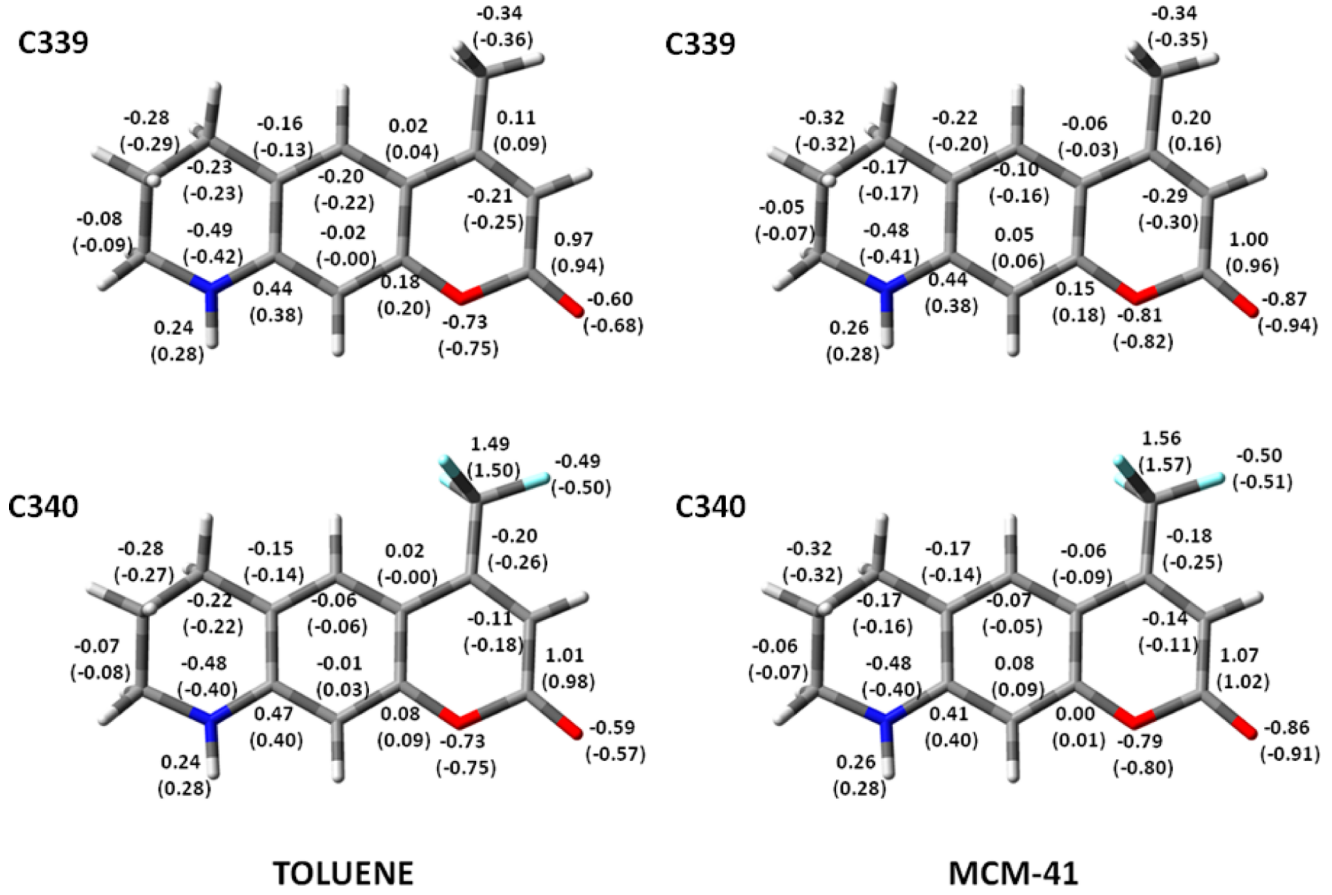

Figure 4. Ground and excited states (the values in parentheses) Mulliken atomic charges of C339 and C340 in toluene solution and adsorbed into MCM-41.

Table 3. Absorption and Emission Wavelengths of C339 and C340 in Vacuum, Toluene, and MCM-41; Computed Oscillator Strengths Are Reported in Parentheses

	abs λ_{max} (nm)		emission λ_{max} (nm)		Stokes shift $\Delta\lambda$ (nm)	
	calcd	exptl	calcd	exptl	calcd	exptl
			coumarin 339			
vacuum	336		368		32	
toluene	354 (0.55)	357	389 (0.55)	409	35	52
MCM-41	376 (0.44)	381	432 (0.27)	444	56	63
			coumarin 340			
vacuum	362		401		39	
toluene	387 (0.55)	386	462 (0.42)	457	75	71
MCM-41	411 (0.50)	409	509 (0.22)	494	98	85

exptl value is 35) and 47 nm (the exptl value is 37), respectively. It is worth highlighting that Li et al.[6] showed that both the absorption and emission spectral shapes of C339 and C340 are very similar to those in toluene. However, the intensity of the emission spectra of the two molecules in MCM-41 decreases dramatically. In agreement with the experimental findings, our calculations show that the oscillator strength (which are reported in parentheses in Table 3) related to the emission spectra for both C339 and C340 are strongly reduced with respect to those relative to the absorption. Indeed, the oscillator strengths of the $S_1 \leftarrow S_0$ transition for the C339/silica assembly is 0.46 and decreases to 0.27 for the $S_1 \rightarrow S_0$ transition. This behavior is not observed with C339 in toluene

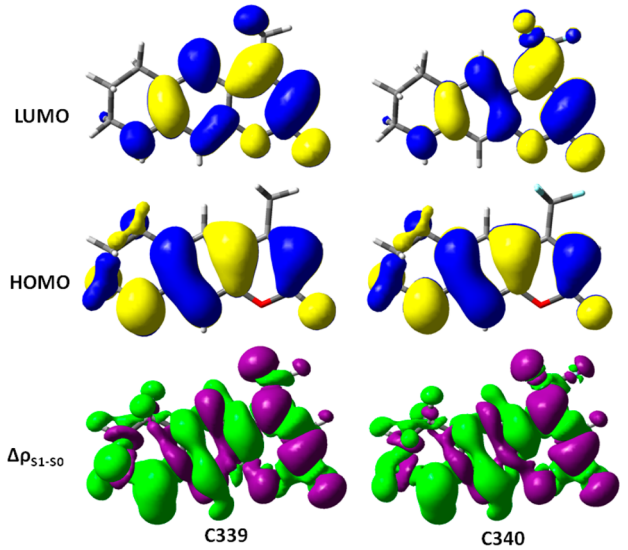

Figure 5. Kohn–Sham MOs involved during the $S_1 \leftarrow S_0$ and the electron density change ($\Delta\rho_{S1-S0}$) upon absorption of light for C339 and C340. Dark violet clouds represent the region where the electron density increases during the transition.

solution, where the calculated oscillator strength remains equal to 0.55 for both $S_1 \leftarrow S_0$ and $S_1 \rightarrow S_0$ transitions, as shown in Table 3. The decrease in emission intensities is due to the relatively strong interaction between the dye molecules and the silica matrix. The carbonyl oxygen atoms of these molecules

dx.doi.org/10.1021/jp305294u | J. Phys. Chem. C 2012, 116, 17807–17818

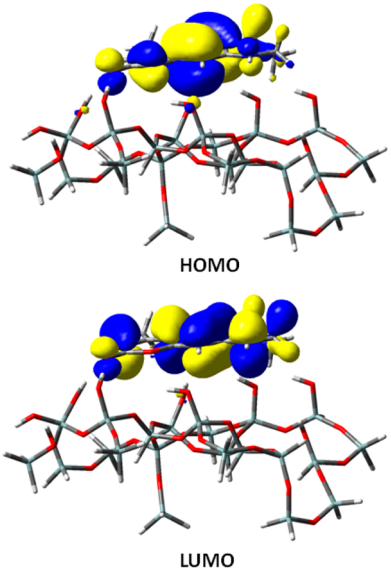

Figure 6. Kohn–Sham MOs involved during the $S_1 \leftarrow S_0$ transition for C339 adsorbed onto the silica surface.

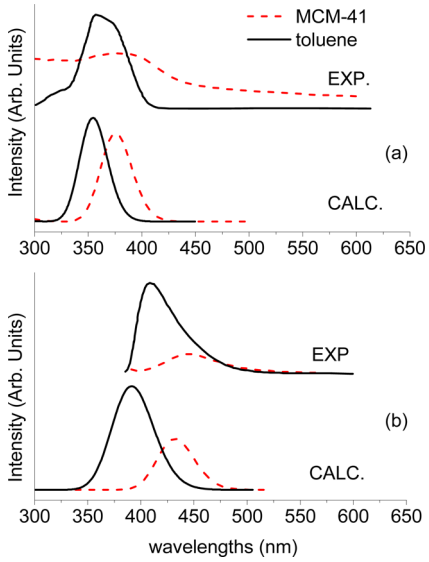

Figure 7. (a) Absorption electronic spectra of C339 in toluene solution (solid black line) and adsorbed on the silica surface (dashed red line) and (b) emission electronic spectra of C339 in toluene solution (solid black line) and adsorbed on the silica surface (dashed red line).

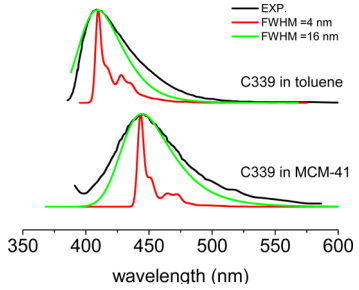

Figure 8. Superposition of computed emission spectra of C339 in toluene (top) and in MCM-41 (bottom) at 298 K with the experimental ones digitized from ref 6.

form strong H-bonds with the silanol groups present on the silica surface of MCM-41. Upon photoexcitation, the H-bonds with the silica surface are significantly changed due to the charge redistribution between the ground and the excited states. The hydrogen bonding dynamics in the excited electronic states can be associated to many photochemical and photophysical phenomena, such as fluorescence quenching, ultrafast internal conversion, intersystem crossing, photo-induced electron transfer, and vibrational energy relaxation.[46,47]

Our calculations show that the frontier orbitals of the dye/silica assembly are very similar to their counterparts in toluene solution, albeit in the former case, the LUMO orbital is very polarized toward the hydrogen atoms of the silanol groups forming the Hb1 and Hb2 hydrogen bonds. Therefore, these interactions lead to an increased charge polarization, causing a decrease in the fluorescence intensity.

Vibrationally Resolved Spectra of C339 in Toluene and in MCM-41. Figure 7 compares the computed purely electronic absorption (panel a) and emission spectra (panel b) of C339 in toluene solution and adsorbed in MCM-41 with their experimental counterparts. Albeit the computed electronic spectra reproduce well both the solvatochromic and Stokes shifts of the dye molecule in toluene and MCM-41, the band shape does not show the right asymmetric tail at longer wavelengths. In order to reproduce correctly the band shape, it is necessary to include the vibrational fine structure associated to the electronic transition as shown in Figure 8. In this figure, the computed vibronic emission spectra of C339 in toluene and MCM-41 are compared to the experimental ones. To highlight the changes of the broadening on the band-shape, the spectra have been scaled so that their highest peak has a height of 1.0. Moreover, the computed spectra have been shifted so that their maxima coincide with the experimental ones. Temperature effects were simulated with the protocol described in ref 10. Using a temperature of 298.15 K, all initial vibrational states with at most 3 simultaneously excited modes and a Boltzmann population greater or equal to 10% of the vibrational ground state's were included in the summation given in eq 2. For C339 in toluene, 326 states were selected with such parameters and 15 163 states for C339 in MCM-41. To keep the computational cost affordable, the threshold on the minimum Boltzmann population was raised to 25% for the latter system, reducing the treatment to 2182 initial states. In order to get a good convergence for C339 in toluene with the prescreening method used for each set of initial states (see ref 10 for details), the maximum number of quanta in class 1, C_1^{max}, was set to 30, the maximum number of quanta for each mode in class 2, C_2^{max}, was set to 20, and the total number of integrals to compute in each class for a given state, N_I^{tot}, was set to 2×10^9. For C339 in MCM-41, the settings were $C_1^{max} = 40$, $C_2^{max} = 30$, $N_I^{tot} = 2 \times 10^9$. The broadening was simulated with Gaussian functions with half-width at half-maxima of 4 and 16 nm, respectively.

The latter broadening results in emission spectra whose band shape asymmetry is very similar to the experimental one, a result that cannot be obtained by broadening purely electronic spectra.

Once demonstrated that vibronic effects must be taken into proper account to simulate reliable band shapes, the analysis of the spectra in terms of vibronic transition assignments for both absorption and emission can be done.

The lower broadening unravels a rich band structure, which is hidden in experimental spectra. From a theoretical point of view, a low broadening is also well-suited to investigate various

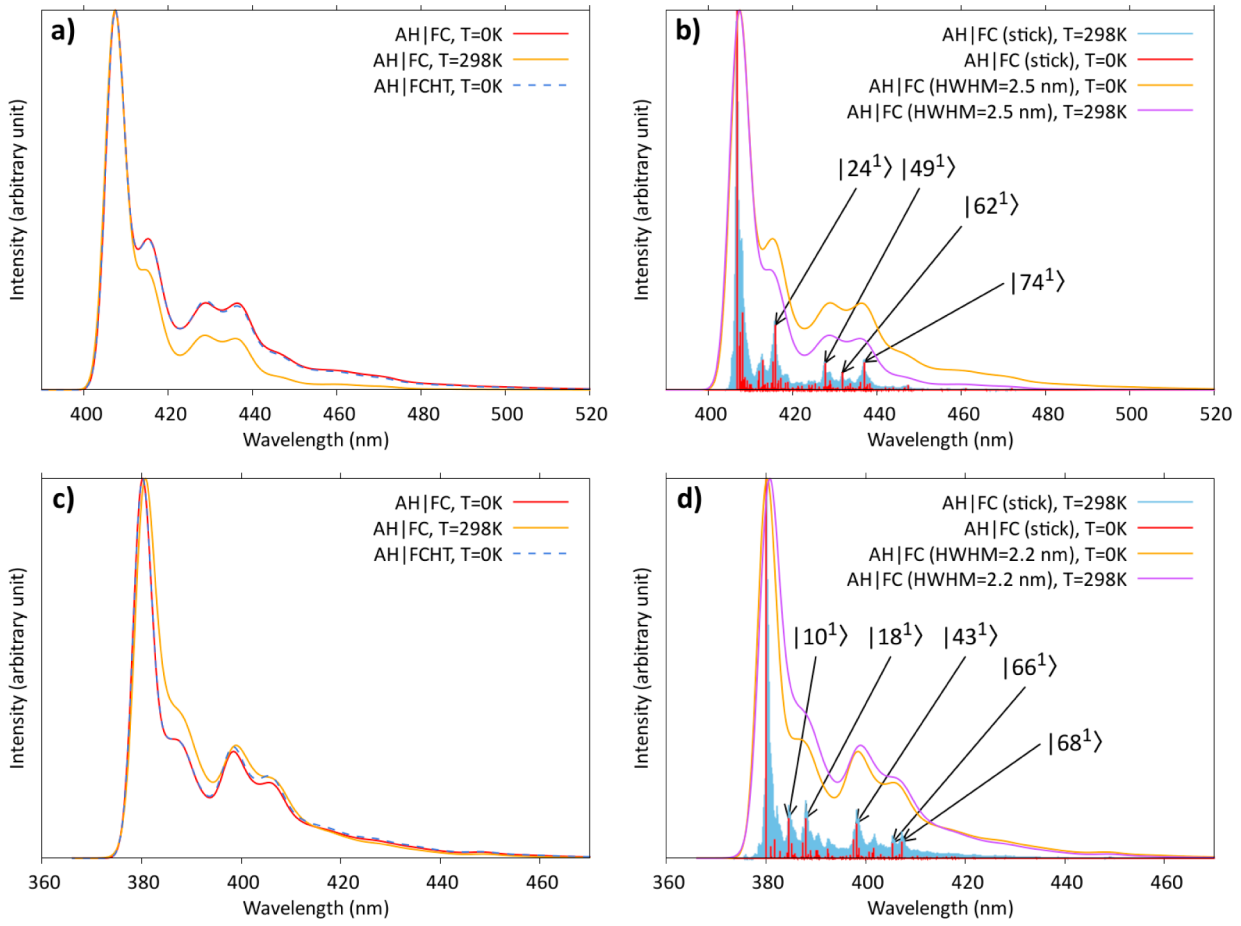

Figure 9. Comparison of temperature and Herzberg−Teller effects on the OPE spectrum of C339 in MCM-41 (a) and in toluene (c). Panels b and d show the stick spectra at T = 0 K and T = 298.15 K for C339 in MCM-41 and in toluene, respectively. Band assignment has been done for transitions from the vibrational ground state, and the ket symbol represents the final vibrational state.

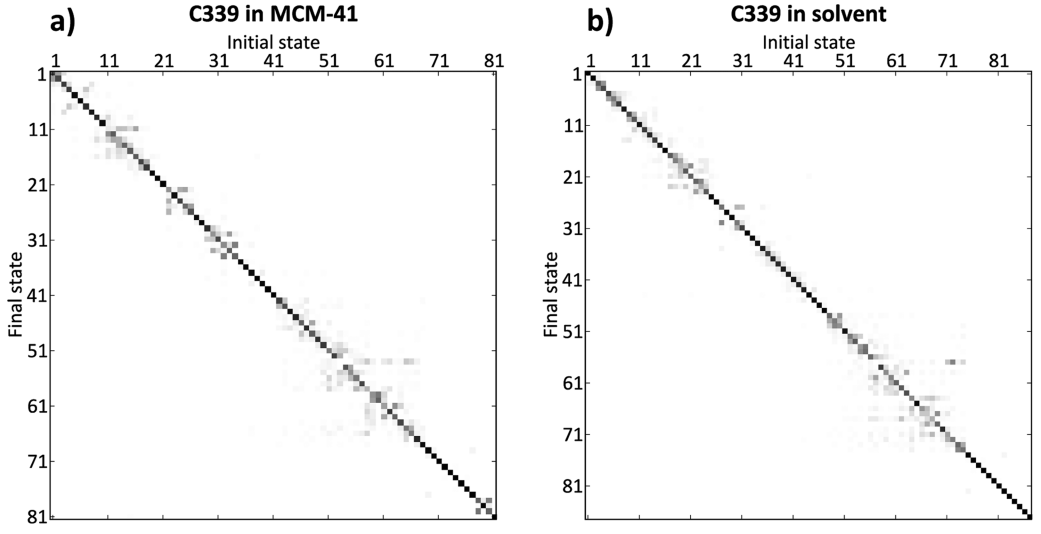

Figure 10. Duschinsky matrixes of C339 in MCM-41 (a) and in toluene (b) for the OPE spectrum. A gray scale is used to represent the magnitude of each element of the matrix, with a white square for a near-null value and a black square for 1.

effects on the band-shape, such as the temperature or the impact of including the Herzberg−Teller term in the Taylor expansion of the electronic dipole transition moment given in eq 3. The resulting OPE spectra of C339 simulated with those effects are shown in panels a and c of Figure 9. While the temperature effects on the band-shape are mostly negligible for C339 in toluene (panel c), we observe a significant change for C339 in MCM-41 (panel a) with an increase of the relative intensity of lower-energy peaks with respect to the transition between the vibrational ground states (left-most, highest peak), in the following labeled "0−0 transition". The same broadening was used for both systems, with a full-width at half-maximum of

dx.doi.org/10.1021/jp305294u | J. Phys. Chem. C 2012, 116, 17807−17818

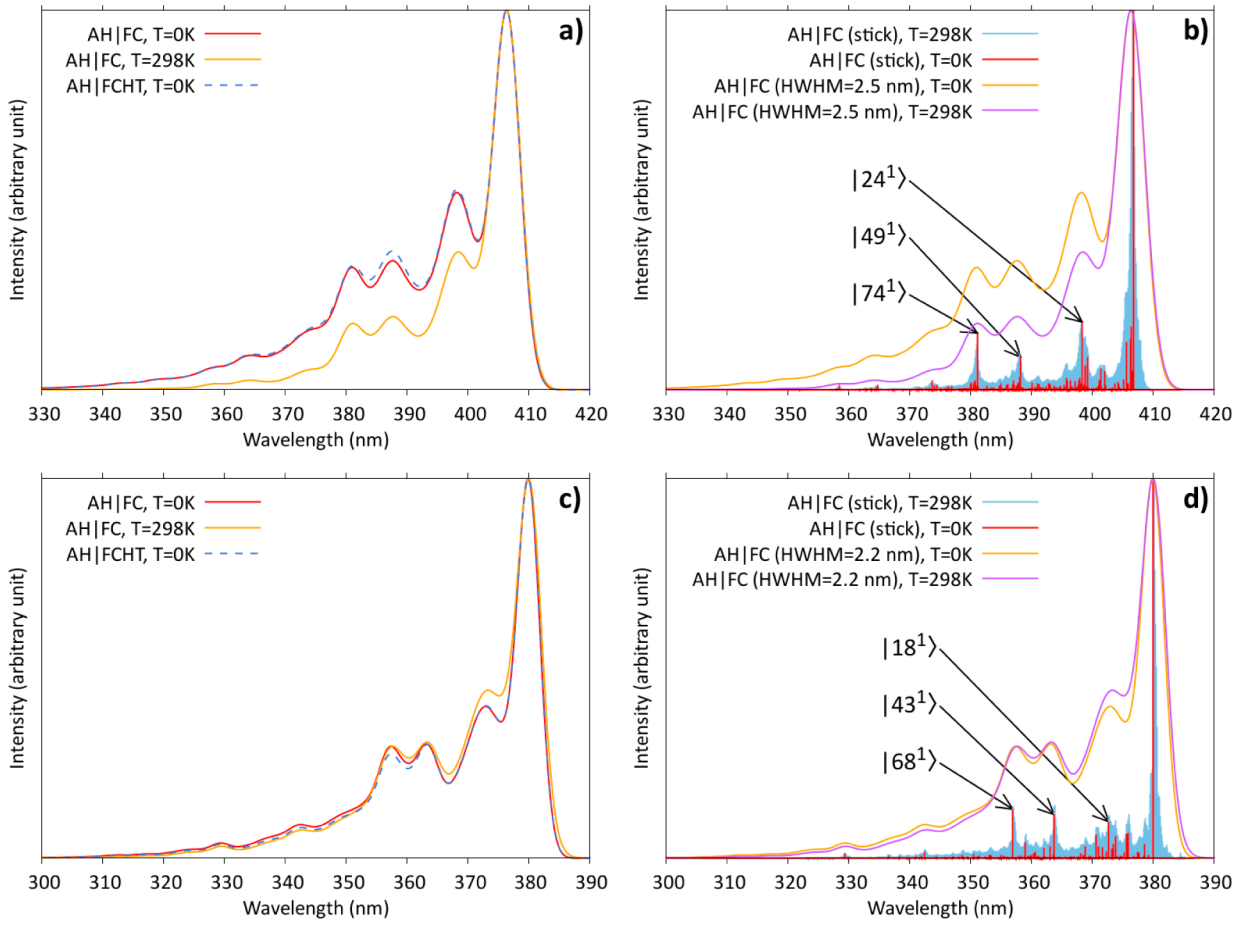

Figure 11. Comparison of temperature and Herzberg−Teller effects on the OPA spectrum of C339 in MCM-41 (a) and in toluene (c). Panels b and d show the stick spectra at T = 0 K and T = 298.15 K for C339 in MCM-41 and in toluene, respectively. Band assignment has been done for transitions from the vibrational ground state, and the ket symbol represents the final vibrational state.

37 meV (150 cm^{-1}), which corresponds to 4.4 nm for C339 in toluene and 5 nm for C339 in MCM-41. Inclusion of the Herzberg−Teller term in the electronic transition dipole moment has no effect on the band-shape, so the latter can be safely studied at the Franck−Condon level. Figure 9b,d shows the stick spectra together with the convoluted spectra at T = 0 K and 298.15 K. For C339 in toluene, the stick spectrum in Figure 9d at T = 298.15 K is composed of a homogeneous repartition of peaks over the energy range, except near the energy of the most intense transitions at T = 0 K where a Gaussian-shaped distribution of peaks is present. Consequently, the scaled, convoluted spectra at T = 0 K and T = 298.15 K are very similar. In both cases, 4 bands can be individuated, although for C339 in toluene, the second band is partly merged in the first one. For the sake of readability and understandability, band assignment in Figure 9d has been limited to the most intense transitions from the ground state $|0\rangle$. The transitions are identified by the final vibrational state represented as a list of all excited modes with their respective number of quanta reported as superscripts. The normal modes are numbered as follows. Those of the lower electronic state are ordered by increasing vibrational energies. The normal modes of the excited states are ordered so that the elements of the Duschinsky matrix with the highest magnitude are placed on its diagonal. The Duschinsky matrixes of C339 in MCM-41 and in toluene are shown in Figure 10. Each element $J(i,k)$ is represented as a square whose color is a shade of gray ranging from white (0.0) to black (1.0) depending on its squared value. For C339 in toluene, the most intense transitions starting from the vibrational ground state are to fundamentals. Mode 10 corresponds to methyl wagging; modes 18, 43, and 66 are ring C═C stretchings; and mode 68 is a C═O stretching. A similar trend is observed for C339 in MCM-41 (Figure 9b). However, the denser bath of transitions leads to noticeable discrepancies between the convoluted spectra at T = 0 K and T = 298.15 K. Considering only transitions from the ground state, the assignment of the 4 main bands is comparable to C339 in toluene, with modes 24 and 49 ring C═C stretchings and mode 74 a C═O stretching, while mode 62 is a bending vibration of the methyl group.

Similar trends are observed for the one-photon absorption spectra, shown in Figure 11. In the same way as OPE, for both C339 in MCM-41 (panel a) and C339 in toluene (panel c), inclusion of the Herzberg−Teller effect has little incidence on the band-shape, whether temperature is taken into account or not, so that the Franck−Condon approximation is sufficient to simulate the one-photon absorption (OPA) spectra. Also, temperature has little effect on the band-shape of the OPA spectrum of C339 in toluene but needs to be taken into account for C339 in MCM-41. Similarly to their OPE counterparts, OPA spectra present 4 bands, albeit more distinguishable here. This latter characteristic is due to the presence of less significant transitions, as revealed from the stick spectra reported in panels b (C339 in MCM-41) and d (C339

dx.doi.org/10.1021/jp305294u | J. Phys. Chem. C 2012, 116, 17807−17818

in toluene) of Figure 11. Indeed, transitions $|0\rangle \rightarrow |62^1\rangle$ for C339 in MCM-41, $|0\rangle \rightarrow |10^1\rangle$ and $|0\rangle \rightarrow |66^1\rangle$ for C339 in toluene are weak in absorption, transitions $|0\rangle \rightarrow |49^1\rangle$ and $|0\rangle \rightarrow |74^1\rangle$ for C339 in MCM-41, $|0\rangle \rightarrow |68^1\rangle$ for C339 in toluene are comparatively more intense with respect to the 0−0 transition. Consequently, 3 transitions from the ground states to fundamentals can be clearly singled out in the absorption spectrum of each system at $T = 0$ K. It is noteworthy that the three modes identified in the band assignments in panels b and d are the same in both systems, so that the main features of the absorption spectrum of isolated coumarin C339 seem unaltered after adsorption on the slab of silica.

CONCLUSIONS

The structural, optical, and electronic properties of C339 and C340 molecular dyes incorporated into MCM-41 have been investigated by employing DFT and TD-DFT calculations.

The structure of both molecules is not heavily deformed when they interact with the silica matrix, the major changes occurring for the C═O bond length, which increases because of the formation of two strong H-bonds between the C═O moiety and two silanol groups at the silica surface. These H-bonds are significantly strengthened upon photoexcitation.

Our results reproduce well the peak positions of the experimental absorption and emission spectra in both toluene and MCM-41.

It has been shown that the inclusion of an electron withdrawing group $-CF_3$ in position 6 of the coumarin molecule subtracts electron density from the carbonyl group, which is responsible for the stabilization of the dye/silica assembly. Therefore, C340 interacts less efficiently than C339 with the silanol groups on the silica surface. However, the mechanism of stabilization is the same, as well as the effect of the silica potential on the optical properties of the coumarin molecules.

Interestingly, the computed oscillator strength related to the emission spectra for both C339 and C340 in MCM-41 are strongly reduced with respect to those of the absorption energies, a behavior that is not observed in toluene and that could be related to charge polarization processes occurring in the excited molecule adsorbed on the silica surface. However, purely electronic spectra do not permit to reproduce well the band shape of the experimental ones, a problem which is overcome by taking into account the vibrational resolution of the transition.

It is noteworthy that the vibronic calculations including temperature effects are very demanding from a computational point of view, especially for large systems such as those investigated in this work. In fact, this is the first time that such calculations have been performed on a dye/silica assembly containing more than 120 atoms.

Finally, a detailed analysis of the band-shape of the absorption and fluorescence spectra of the C339 molecule has been carried out in terms of vibronic transitions with particular emphasis on the influence of the silica matrix on the band-shape.

ASSOCIATED CONTENT

Supporting Information

Analysis of the reliability of the reduced-dimensionality scheme used to model the C339/silica assembly in reproducing the internal vibrations of C339 compared to the full representation. This material is available free of charge via the Internet at http://pubs.acs.org.

AUTHOR INFORMATION

Corresponding Author

*E-mail: apedone@unimo.it.

Notes

The authors declare no competing financial interest.

ACKNOWLEDGMENTS

A.P. thanks professor Piero Ugliengo (University of Turin) who kindly provided the MCM-41 structural model used in this work.

REFERENCES

(1) Schulz-Ekloff, G.; Wöhrle, D.; van Duffel, B.; Schoonheydt, R. A. *Microporous Mesoporous Mater.* **2002**, *51*, 91−138.
(2) Herz, E.; Marchincin, T.; Connelly, L.; Bonner, D.; Burns, A.; Switalski, S.; Wiesner, U. *J. Fluoresc.* **2009**, *20*, 67−72.
(3) Kresge, C. T.; Leonowicz, M. E.; Roth, W. J.; Vartuli, J. C.; Beck, J. S. *Nature* **1992**, *359*, 710−712.
(4) Xu, W.; Guo, H. Q.; Akins, D. L. *J. Phys. Chem. B* **2001**, *105*, 7686−7689.
(5) Gu, G.; Ong, P. P.; Li, Q. *J. Phys. D: Appl. Phys.* **1999**, *32*, 2287−2289.
(6) Li, D.; Zhao, W.; Sun, X.; Zhang, J.; Anpo, M.; Zhao, J. *Dyes Pigm.* **2006**, *68*, 33−37.
(7) Yao, Y. F.; Zhang, M. S.; Shi, J. X.; Gong, M. L.; Zhang, H. J.; Yang, Y. S. *Mater. Lett.* **2001**, *48*, 44−48.
(8) Barone, V.; Bloino, J.; Biczysko, M.; Santoro, F. *J. Chem. Theory Comput.* **2009**, *5*, 540−554.
(9) Improta, R.; Barone, V.; Santoro, F. *Angew. Chem., Int. Ed.* **2007**, *46*, 405−408.
(10) Bloino, J.; Biczysko, M.; Santoro, F.; Barone, V. *J. Chem. Theory Comput.* **2010**, *6*, 1256−1274.
(11) Santoro, F.; Improta, R.; Lami, A.; Bloino, J.; Barone, V. *J. Chem. Phys.* **2007**, *126*, 084509.
(12) Pedone, A.; Prampolini, G.; Monti, S.; Barone, V. *Phys. Chem. Chem. Phys.* **2011**, *13*, 16689−16697.
(13) Pedone, A.; Prampolini, G.; Monti, S.; Barone, V. *Chem. Mater.* **2011**, *23*, 5016−5023.
(14) Dreuw, A.; Head-Gordon, M. *Chem. Rev.* **2005**, *105*, 4009−4037.
(15) Tomasi, J.; Mennucci, B.; Cammi, R. *Chem. Rev.* **2005**, *105*, 2999−3094.
(16) Tabacchi, G.; Fois, E.; Calzaferri, G. *J. Phys. Chem. C* **2010**, *114*, 10572−10579.
(17) De Angelis, F.; Tilocca, A.; Selloni, A. *J. Am. Chem. Soc.* **2004**, *126*, 15024−15025.
(18) Sánchez-de-Armas, R.; San Miguel, M. A.; Oviedo, J.; Fdez Sanz, J. *Phys. Chem. Chem. Phys.* **2012**, *14*, 225−233.
(19) Labat, F.; Ciofini, I.; Hratchian, H. P.; Frisch, M. J.; Raghavachari, K.; Adamo, C. *J. Am. Chem. Soc.* **2009**, *131*, 14290−14298.
(20) Pedone, A.; Biczysko, M.; Barone, V. *ChemPhysChem* **2010**, *11*, 1812−1832.
(21) Barone, V.; Bloino, J.; Monti, S.; Pedone, A.; Prampolini, G. *Phys. Chem. Chem. Phys.* **2010**, *12*, 10550−10561.
(22) Barone, V.; Bloino, J.; Monti, S.; Pedone, A.; Prampolini, G. *Phys. Chem. Chem. Phys.* **2011**, *13*, 2160−2166.
(23) Frisch, M. J.; Trucks, G. W.; Schlegel, H. B.; Scuseria, G. E.; Robb, M. A.; Cheeseman, J. R.; Scalmani, G.; Barone, V.; Mennucci, B.; Petersson, G. A.; Nakatsuji, H.; Caricato, M.; Li, X.; Hratchian, H. P.; Izmaylov, A. F.; Bloino, J.; Zheng, G.; Sonnenberg, J. L.; Hada, M.; Ehara, M.; Toyota, K.; Fukuda, R.; Hasegawa, J.; Ishida, M.; Nakajima, T.; Honda, Y.; Kitao, O.; Nakai, H.; Vreven, T.; Montgomery, J. A., Jr.; Peralta, J. E.; Ogliaro, F.; Bearpark, M.; Heyd, J. J.; Brothers, E.; Kudin,

K. N.; Staroverov, V. N.; Kobayashi, R.; Normand, J.; Raghavachari, K.; Rendell, A.; Burant, J. C.; Iyengar, S. S.; Tomasi, J.; Cossi, M.; Rega, N.; Millam, J. M.; Klene, M.; Knox, J. E.; Cross, J. B.; Bakken, V.; Adamo, C.; Jaramillo, J.; Gomperts, R.; Stratmann, R. E.; Yazyev, O.; Austin, A. J.; Cammi, R.; Pomelli, C.; Ochterski, J. W.; Martin, R. L.; Morokuma, K.; Zakrzewski, V. G.; Voth, G. A.; Salvador, P.; Dannenberg, J. J.; Dapprich, S.; Daniels, A. D.; Farkas, O.; Foresman, J. B.; Ortiz, J. V.; Cioslowski, J.; Fox, D. J. *Gaussian 09*, revision A.01; Gaussian, Inc.: Wallingford, CT, 2009.

(24) Becke, A. D. *J. Chem. Phys.* **1993**, *98*, 5648−5652.

(25) Lee, C.; Yang, W.; Parr, R. G. *Phys. Rev. B* **1988**, *37*, 785−789.

(26) Barone, V.; Cimino, P. *Chem. Phys. Lett.* **2008**, *454*, 139−143.

(27) Curutchet, C.; Scholes, G. D.; Mennucci, B.; Cammi, R. *J. Phys. Chem. B* **2007**, *111*, 13253−13265.

(28) Iozzi, F.; Mennucci, B.; Tomasi, J.; Cammi, R. *J. Chem. Phys.* **2004**, *120*, 7029−7040.

(29) Pedone, A.; Barone, V. *Phys. Chem. Chem. Phys.* **2010**, *12*, 2722−2729.

(30) Improta, R.; Scalmani, G.; Frisch, M.; Barone, V. *J. Chem. Phys.* **2007**, *127*, 074504.

(31) Improta, R.; Barone, V.; Scalmani, G.; Frisch, M. *J. Chem. Phys.* **2006**, *125*, 054103.

(32) Vreven, T.; Mennucci, B.; da Silva, C. O.; Morokuma, K.; Tomasi, J. *J. Chem. Phys.* **2001**, *115*, 62−72.

(33) Ugliengo, P.; Sodupe, M.; Musso, F.; Bush, I. J.; Orlando, R.; Dovesi, R. *Adv. Mater.* **2008**, *20*, 4579−4583.

(34) *Handbook of Glass Properties*; Bansal, N. P., Doremus, R. H., Eds.; Academic Press, Inc.: New York, 1986.

(35) Macak, P.; Luo, Y.; Ågren, H. *Chem. Phys. Lett.* **2000**, *330*, 447−456.

(36) Hazra, A.; Chang, H. H.; Nooijen, M. *J. Chem. Phys.* **2004**, *121*, 2125.

(37) Bloino, J.; Biczysko, M.; Crescenzi, M.; Barone, V. *J. Chem. Phys.* **2008**, *128*, 244105.

(38) Tonge, N. M.; MacMahon, E. C.; Pugliesi, I.; Cockett, M. C. R. *J. Chem. Phys.* **2007**, *126*, 154319.

(39) de Groot, M.; Buma, W. J. *Chem. Phys. Lett.* **2007**, *435*, 224−229.

(40) de Groot, M.; Buma, W. J. *Chem. Phys. Lett.* **2006**, *420*, 459−464.

(41) Diercksen, M.; Grimme, S. *J. Chem. Phys.* **2004**, *120*, 3544.

(42) Pugliesi, I.; Tonge, N. M.; Hornsby, K. E.; Cockett, M. C. R.; Watkins, M. J. *Phys. Chem. Chem. Phys.* **2007**, *9*, 5436−5445.

(43) Miao, C.; Shi, Y. *J. Comput. Chem.* **2011**, *32*, 3058−3061.

(44) Zhao, G. J.; Han, K.-L. *J. Phys. Chem. A* **2007**, *111*, 2469−2474.

(45) Zhao, G. J.; Han, K.-L. *ChemPhysChem* **2008**, *9*, 1842−1846.

(46) Zhao, G. J.; Han, K.-L. *J. Phys. Chem. A* **2009**, *113*, 14329−14335.

(47) Zhang, H. J.; Smith, S. C. *J. Theor. Comput. Chem.* **2007**, *6*, 789−802.